Mon. Not. R. Astron. Soc. **376,** 1621–1629 (2007) doi:10.1111/j.1365-2966.2007.11573.x

Structural parameters of Mayall II = G1 in M31

J. Ma,[1⋆] R. de Grijs,[2,1] D. Chen,[1] S. van den Bergh,[3] Z. Fan,[1,4] Z. Wu,[1] H. Wu,[1] X. Zhou,[1] J. Wu,[1] Z. Jiang[1] and J. Chen[1]

[1]*National Astronomical Observatories, Chinese Academy of Sciences, Beijing 100012, China*
[2]*Department of Physics & Astronomy, The University of Sheffield, Hicks Building, Hounsfield Road, Sheffield S3 7RH*
[3]*Dominion Astrophysical Observatory, Herzberg Institute of Astrophysics, National Research Council, 5071 West Saanich Road, Victoria, Canada BC V9E 2E7*
[4]*Graduate University of Chinese Academy of Sciences, A19 Yuquan Road, Shijingshan District, Beijing 100049, China*

Accepted 2007 January 31. Received 2007 January 30; in original form 2006 August 25

ABSTRACT

Mayall II = G1 is one of the most luminous globular clusters (GCs) known in M31. New deep, high-resolution observations with the Advanced Camera for Surveys on the *Hubble Space Telescope* are used to provide accurate photometric data to the smallest radii yet. In particular, we present the precise variation of ellipticity and position angle, and of surface brightness for the core of the object. Based on these accurate photometric data, we redetermine the structural parameters of G1 by fitting a single-mass isotropic King model. We derive a core radius, $r_c = 0.21 \pm 0.01$ arcsec ($= 0.78 \pm 0.04$ pc), a tidal radius, $r_t = 21.8 \pm 1.1$ arcsec ($= 80.7 \pm 3.9$ pc), and a concentration index $c = \log(r_t/r_c) = 2.01 \pm 0.02$. The central surface brightness is 13.510 mag arcsec^{-2}. We also calculate the half-light radius, at $r_h = 1.73 \pm 0.07$ arcsec ($= 6.5 \pm 0.3$ pc). The results show that, within 10 core radii, a King model fits the surface brightness distribution well. We find that this object falls in the same region of the M_V versus log R_h diagram as ω Centauri, M54 and NGC 2419 in the Milky Way. All three of these objects have been claimed to be the stripped cores of now defunct dwarf galaxies. We discuss in detail whether GCs, stripped cores of dwarf spheroidals and normal dwarf galaxies form a continuous distribution in the M_V versus log R_h plane, or if GCs and dwarf spheroidals constitute distinct classes of objects; we present arguments in favour of this latter view.

Key words: globular clusters: individual: Mayall II = G1 – galaxies: evolution – galaxies: individual: M31.

1 INTRODUCTION

Globular clusters (GCs) are effective laboratories for studying stellar evolution and stellar dynamics. They are ancient building blocks of galaxies, and can help us to understand the formation and evolution of their parent galaxies. In addition, GCs exhibit surprisingly uniform properties, suggesting a common formation mechanism. The density distributions of most of them are well fitted by empirical models of King (1962). The closest other populous GC system beyond the halo of our Galaxy is that of M31. The Andromeda galaxy is the ideal nearby target for studying GCs, since it contains more GCs than all other Local Group galaxies combined (Battistini et al. 1987; Harris 1991; Racine 1991; Fusi Pecci et al. 1993).

The brightest GCs in M31 are more luminous than ω Centauri, which is the most luminous Galactic GC. Among these giants is Mayall II = G1 (hereafter referred to as G1 for reasons of brevity), which was first identified as a GC candidate ('Mayall II') by Mayall & Eggen (1953) using a Palomar 48-inch Schmidt plate taken in 1948. It was subsequently named G1 by Sargent et al. (1977) in their survey with the Kitt Peak 4-m Mayall telescope of GCs in 29 fields surrounding M31. It is located in the halo of M31, at a projected distance of about 40 kpc from the galaxy's nucleus (see Meylan et al. 2001). This cluster has been studied in detail by Pritchet & van den Bergh (1984), Rich et al. (1996), Meylan et al. (2001) and Barmby, Holland & Huchra (2002), who found that it is quite flattened, with $\epsilon \simeq 0.2$. G1 is also of interest because it may contain a central intermediate-mass ($\sim 2 \times 10^4$ M$_\odot$) black hole (Gebhardt, Rich & Ho 2002, 2005). Meylan et al. (2001) have pointed out that G1 is, following ω Centauri, only the second GC in which convincing evidence for a real abundance dispersion has been seen (although M22 and M54 are also two good candidates for a metallicity spread; see for reviews of Sarajedini & Layden 1995; Da Costa & Armandroff 1995; Monaco et al. 2004). It has therefore been considered as the possible remnant core of a dwarf galaxy which lost most of its envelope through tidal interactions with M31 (Meylan & Heggie 1997; Meylan et al. 2001). Subsequently Mackey & van den Bergh (2005) strengthened the Meylan & Heggie (1997) and Meylan et al. (2001) conclusion.

⋆E-mail: majun@vega.bac.pku.edu.cn

Gebhardt et al. (2005) used the image obtained with the Advanced Camera for Surveys (ACS) on the *Hubble Space Telescope* (*HST*) (in fact, it is the very same image used in this paper) to construct a radial profile of G1, which was fitted by a non-parametric, spherical, isotropic model to examine whether or not G1 contains a central massive black hole. By deconvolving this better spatial resolution image, Gebhardt et al. (2005) found a bright star near the centre of G1, which could not be detected in previous poorer resolution *HST*/Wide Field and Planetary Camera-2 (WFPC2) images. Therefore, the structural parameters of G1 obtained based on this better spatial resolution image will certainly affect previous results based on the poorer resolution *HST*/WFPC2 image. This is one of the key contributions of the present paper.

In this paper, we redetermine the structural parameters of G1 using a deep *HST*/ACS image. This is at the highest resolution yet with which this cluster has been observed; it allows us to both probe the cluster's structure to smaller radii than ever before and obtain the most accurate surface brightness profile at large radii to date.

2 OBSERVATIONS AND DATA REDUCTIONS

2.1 Observations and photometric data

We searched the *HST* archive and found G1 to have been observed with the ACS/High-Resolution Channel (HRC) in the F555W band (equivalent to the Johnson *V* filter) on 2003 October 24, as part of programme GO-9767 (PI Gebhardt). The total integration time was 41 min over six exposures at three positions. Upon retrieval from the STScI archive, all images were processed by the standard ACS calibration pipeline, in which bias and dark subtractions, flat-field division, and the masking of known bad pixels are included. Subsequently, photometric header keywords are populated. In the final stage of the pipeline, the MULTIDRIZZLE software is used to correct the geometric distortion present in the HRC images. Finally, any cosmic rays are rejected while individual images are combined into a final single image with an exposure time of 2460 s (see Fig. 1).

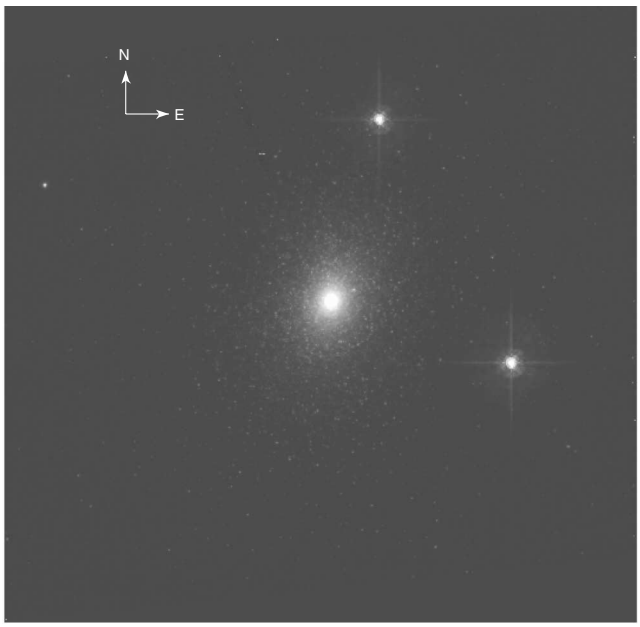

Figure 1. Image of Mayall II = G1 observed with the *HST*/ACS in the F555W band. The high resolution of 0.025 arcsec pixel^{-1} makes two bright foreground stars appear far away from the cluster. The image size is 29.25 × 28.55 arcsec^2.

The products obtained from the STScI archive are calibrated drizzled images, in units of counts per second. We checked the images, and did not find saturated cluster stars.

During on-orbit operations, *HST* CCD instruments are subject to radiation damage that degrades their ability to transfer charges. Charge transfer efficiency (CTE) degradation can lead to photometric inaccuracy (see detailed discussions in Riess & Mack 2004; Sirianni et al. 2005). However, in this paper, we did not correct for CTE for the following reasons: (i) in the image used in this paper, charge excesses streaming from the stellar point sources (equivalent to the effects of bleeding, although at a much lower flux level) are not detected, that is, corrections for CTE are not significant; (ii) as Sirianni et al. (2005) pointed out, monitoring CTE degradation is fairly easy, but the calculation of a correction formula is more difficult. In fact, until now, only Riess (2003) and Riess & Mack (2004) provided correction formulae to correct photometric losses as a function of a source's position, flux, background, time and aperture size on the ACS WFC CCDs. Gebhardt et al. (2005) did not correct for CTE effects either in their analysis of the same image used in this paper.

The ACS/HRC spatial resolution is 0.025 arcsec pixel^{-1}. This high resolution makes two bright foreground stars appear far away from the cluster, and hence is helpful to obtain accurate photometry of the cluster. We used the IRAF task ellipse to fit the image with a series of elliptical annuli from the centre to the outskirts, with the length of the semimajor axis increasing in steps of 8 per cent. The centre coordinates of the isophotes were fixed. For our photometry, we derived the background value as the mean of a region of 100 × 100 pixels in the lower left-hand corner of the image, the centre of which was taken 779 pixel away from the cluster centre, and masked three areas, which were found to be disturbed by three foreground stars. We checked the image carefully, and did not find other obvious foreground stars. There are no obvious background galaxies, judging from the brightnesses and extent of the objects in the field of view. We performed the photometric calibration using the results of Sirianni et al. (2005). Magnitudes are derived in the ACS/HRC VEGAMAG system. The relevant zero-point for this system is 25.255 in F555W magnitudes (Sirianni et al. 2005).

2.2 Ellipticity and position angle

Table 1 gives the ellipticity, $\epsilon = 1 - b/a$, and the position angle (PA) as a function of the semimajor axis length, a, from the centre of annulus. PAs are measured anticlockwise from the vertical axis in Fig. 1. These observables have also been plotted in Fig. 2; the errors were generated by the IRAF task ellipse, in which the ellipticity errors are obtained from the internal errors in the harmonic fit, after removal of the first and second fitted harmonics. Beyond $a =$ 7.385 arcsec, the ellipticity and PA could not be obtained unambiguously, that is, the fits did not converge because of the low signal-to-noise ratio at those large radii. The mean ellipticity is $\epsilon \simeq 0.19$, which is in good agreement with the $\epsilon \simeq 0.2$ of Meylan et al. (2001). The ellipticity varies significantly as a function of the cluster's semimajor axis, from a minimum of $\epsilon = 0.05$ at $a \sim 0.2$ arcsec to a maximum $\epsilon = 0.32$ at $a \sim 2.9$ arcsec. This is, to within the observational uncertainties, similar to the results of Meylan et al. (2001), whose data points are also included in Fig. 1 for a direct comparison (open circles). It is clear that while the general trend of the cluster's ellipticity as a function of semimajor axis radius is similar between the *HST*/WFPC2-based data of Meylan et al. (2001), the improved spatial resolution of our new *HST*/ACS data allows us to probe this trend deeper into the cluster core. Fig. 2 clearly shows that in the

Table 1. G1: ellipticity, ϵ, and PA as a function of the semimajor axis, a.

a (arcsec)	ϵ	PA (°)	a (arcsec)	ϵ (°)	PA
0.039	0.238 ± 0.028	144.5 ± 3.9	0.583	0.137 ± 0.013	110.4 ± 2.8
0.043	0.230 ± 0.027	143.1 ± 3.9	0.629	0.182 ± 0.011	107.2 ± 2.0
0.046	0.225 ± 0.026	142.2 ± 3.8	0.680	0.220 ± 0.009	104.4 ± 1.3
0.050	0.217 ± 0.025	142.9 ± 3.9	0.734	0.226 ± 0.009	105.6 ± 1.3
0.054	0.211 ± 0.022	145.0 ± 3.5	0.793	0.205 ± 0.013	110.0 ± 2.1
0.058	0.192 ± 0.023	142.9 ± 4.0	0.856	0.218 ± 0.013	110.4 ± 1.9
0.063	0.194 ± 0.026	143.5 ± 4.3	0.925	0.171 ± 0.011	111.2 ± 2.0
0.068	0.186 ± 0.031	142.9 ± 5.6	0.999	0.181 ± 0.018	111.2 ± 3.2
0.073	0.172 ± 0.034	139.8 ± 6.3	1.078	0.205 ± 0.016	111.2 ± 2.5
0.079	0.163 ± 0.037	138.7 ± 7.1	1.165	0.272 ± 0.013	107.9 ± 1.5
0.085	0.164 ± 0.038	137.6 ± 7.4	1.258	0.264 ± 0.022	110.7 ± 2.8
0.092	0.165 ± 0.038	132.1 ± 7.2	1.358	0.264 ± 0.026	110.7 ± 3.3
0.099	0.169 ± 0.037	126.5 ± 7.1	1.467	0.180 ± 0.015	110.7 ± 2.6
0.107	0.160 ± 0.035	125.6 ± 6.9	1.585	0.234 ± 0.017	108.6 ± 2.4
0.116	0.154 ± 0.031	126.0 ± 6.3	1.711	0.234 ± 0.018	108.6 ± 2.4
0.125	0.148 ± 0.030	125.5 ± 6.4	1.848	0.272 ± 0.011	99.6 ± 1.4
0.135	0.145 ± 0.031	125.5 ± 6.7	1.996	0.272 ± 0.021	103.5 ± 2.6
0.146	0.154 ± 0.031	126.0 ± 6.3	2.156	0.272 ± 0.017	103.5 ± 2.0
0.157	0.149 ± 0.027	126.6 ± 5.7	2.328	0.272 ± 0.019	103.5 ± 2.3
0.170	0.140 ± 0.021	122.8 ± 4.7	2.514	0.272 ± 0.032	103.5 ± 3.9
0.184	0.121 ± 0.019	120.4 ± 4.6	2.716	0.272 ± 0.019	109.0 ± 2.3
0.198	0.078 ± 0.019	114.9 ± 7.2	2.933	0.324 ± 0.011	110.2 ± 1.2
0.214	0.046 ± 0.019	103.9 ± 12.0	3.167	0.256 ± 0.019	104.7 ± 2.5
0.231	0.051 ± 0.017	104.0 ± 9.9	3.421	0.208 ± 0.017	106.5 ± 2.6
0.250	0.074 ± 0.016	112.5 ± 6.6	3.695	0.276 ± 0.024	107.3 ± 2.9
0.270	0.092 ± 0.015	116.6 ± 4.8	3.990	0.275 ± 0.025	117.5 ± 3.0
0.291	0.103 ± 0.014	114.3 ± 4.1	4.309	0.268 ± 0.031	112.3 ± 3.8
0.315	0.123 ± 0.013	106.4 ± 3.2	4.654	0.263 ± 0.028	107.1 ± 3.5
0.340	0.137 ± 0.011	102.1 ± 2.4	5.026	0.256 ± 0.016	109.1 ± 2.1
0.367	0.151 ± 0.011	101.2 ± 2.3	5.428	0.256 ± 0.019	109.1 ± 2.5
0.397	0.151 ± 0.013	99.0 ± 2.7	5.863	0.249 ± 0.023	113.4 ± 3.1
0.428	0.147 ± 0.019	98.6 ± 3.9	6.332	0.240 ± 0.034	113.4 ± 4.7
0.463	0.120 ± 0.018	109.9 ± 4.7	6.838	0.164 ± 0.020	118.8 ± 3.8
0.500	0.124 ± 0.012	111.0 ± 3.0	7.385	0.192 ± 0.030	120.1 ± 5.0
0.539	0.136 ± 0.012	112.7 ± 2.7			

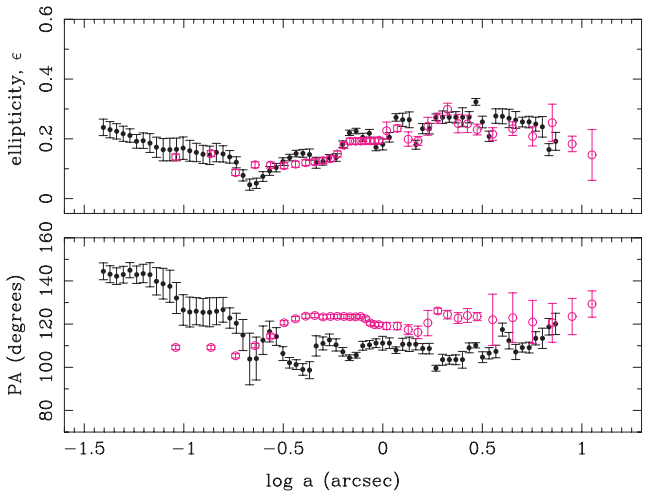

Figure 2. Ellipticity and PA as a function of the semimajor axis. The filled circles are our measurements in this paper; the open circles are from Meylan et al. (2001).

inner parts ($a < 0.2$ arcsec) the ellipticity increases towards smaller semimajor axis radii. This figure also shows that uncertainties in the exact value of the PA are only of secondary importance for the general trend in ellipticity observed, given that the PA determination between Meylan et al. (2001) and the present paper differs by $\lesssim 10^\circ$. There are a number of possible reasons for the offsets in PA observed between these two studies, including those related to the accuracy of the centring of our isophotes (which is linked to the different pixel sizes), and the steps in semimajor axis radius adopted, among others. It is of interest to note that the high ellipticity of G1 supports the empirical rule of van den Bergh (1996) that the brightest GCs in a galaxy are also usually the most flattened ones. The most luminous GC in M31, 037-B327, also has a high ellipticity, of $\epsilon \simeq 0.23$ (see Ma et al. 2006), while the vast majority of M31 GCs have ellipticities close to a median $\epsilon = 0.10$ (e.g. Lupton 1989; Staneva, Spassova & Golev 1996; D'Onofrio et al. 1994; Barmby, Holland & Huchra 2002), although some of the faintest M31 GCs show significant flattening as well (Barmby et al. 2002). The PA of the major axis is not significantly variable for semimajor axis values $a > \sim 0.2$ arcsec, in agreement with Meylan et al. (2001). However, just as for the ellipticity, the PA also increases towards smaller semimajor axis radii for $a < 0.2$ arcsec.

2.3 Surface brightness profile and King model fits

After elliptical galaxies, GCs are the best understood and most thoroughly modelled class of stellar systems. For example, a large majority of the ∼150 Galactic GCs have been fitted by the simple models of single-mass, isotropic, lowered isothermal spheres developed by

Table 2. G1: surface brightness, μ, and integrated magnitude, m, as a function of the radius in the F555 band.

R (arcsec)	μ (mag)	m (mag)	R (arcsec)	μ (mag)	m (mag)
0.039	13.525 ± 0.001	19.123	0.856	16.401 ± 0.005	14.583
0.043	13.536 ± 0.001	19.123	0.925	16.684 ± 0.004	14.536
0.046	13.549 ± 0.001	19.123	0.999	16.849 ± 0.005	14.484
0.050	13.564 ± 0.001	19.123	1.078	16.943 ± 0.005	14.433
0.054	13.580 ± 0.001	18.752	1.165	16.997 ± 0.005	14.383
0.058	13.600 ± 0.001	18.262	1.258	17.145 ± 0.008	14.335
0.063	13.618 ± 0.001	18.262	1.358	17.304 ± 0.011	14.292
0.068	13.639 ± 0.001	18.262	1.467	17.647 ± 0.005	14.253
0.073	13.664 ± 0.002	18.089	1.585	17.743 ± 0.006	14.214
0.079	13.691 ± 0.002	17.947	1.711	17.904 ± 0.007	14.178
0.085	13.717 ± 0.002	17.711	1.848	17.998 ± 0.006	14.142
0.092	13.746 ± 0.002	17.524	1.996	18.271 ± 0.007	14.108
0.099	13.777 ± 0.003	17.524	2.156	18.426 ± 0.007	14.075
0.107	13.815 ± 0.003	17.243	2.328	18.618 ± 0.006	14.043
0.116	13.857 ± 0.002	17.129	2.514	18.815 ± 0.008	14.014
0.125	13.901 ± 0.002	16.986	2.716	18.970 ± 0.007	13.986
0.135	13.945 ± 0.003	16.825	2.933	19.029 ± 0.007	13.960
0.146	13.986 ± 0.003	16.723	3.167	19.511 ± 0.006	13.936
0.157	14.038 ± 0.003	16.635	3.421	19.688 ± 0.009	13.915
0.170	14.100 ± 0.003	16.481	3.695	19.856 ± 0.007	13.894
0.184	14.177 ± 0.003	16.319	3.990	19.992 ± 0.013	13.873
0.198	14.276 ± 0.003	16.250	4.309	20.236 ± 0.012	13.855
0.214	14.373 ± 0.003	16.104	4.654	20.471 ± 0.011	13.838
0.231	14.455 ± 0.003	15.975	5.026	20.615 ± 0.010	13.821
0.250	14.529 ± 0.003	15.906	5.428	20.942 ± 0.014	13.804
0.270	14.612 ± 0.003	15.781	5.863	21.322 ± 0.011	13.791
0.291	14.705 ± 0.002	15.684	6.332	21.391 ± 0.016	13.778
0.315	14.783 ± 0.003	15.576	6.838	21.735 ± 0.018	13.766
0.340	14.876 ± 0.003	15.482	7.385	21.930 ± 0.022	13.755
0.367	14.984 ± 0.003	15.391	7.976	22.491 ± 0.015	13.746
0.397	15.114 ± 0.003	15.296	8.614	22.862 ± 0.012	13.736
0.428	15.248 ± 0.004	15.205	9.303	22.639 ± 0.028	13.727
0.463	15.362 ± 0.004	15.123	10.048	22.924 ± 0.020	13.718
0.500	15.474 ± 0.003	15.051	10.851	23.126 ± 0.028	13.708
0.539	15.595 ± 0.004	14.971	11.720	23.500 ± 0.022	13.700
0.583	15.756 ± 0.003	14.901	12.657	23.798 ± 0.018	13.693
0.629	15.845 ± 0.003	14.831	13.670	23.736 ± 0.021	13.685
0.680	15.934 ± 0.003	14.765	14.763	23.992 ± 0.029	13.678
0.734	16.101 ± 0.003	14.702	15.944	24.476 ± 0.040	13.674
0.793	16.290 ± 0.004	14.642	17.220	24.704 ± 0.049	13.670

Michie (1963) and King (1966) (hereafter 'King models'), yielding comprehensive catalogues of cluster structural parameters and physical properties (see McLaughlin & van der Marel 2005, and references therein). For extragalactic GCs, *HST* imaging data have been used to fit King models to a large number of GCs in M31 (e.g. Barmby et al. 2002, and references therein), four GCs in M33 (Larsen et al. 2002), and also a few GCs in NGC 5128 (e.g. Harris et al. 2002, and references therein).

Table 2 lists the surface brightness, μ, of G1, and its integrated magnitude, m, as a function of radius. The errors in the surface brightness were also generated by the IRAF task ellipse, in which they are obtained directly from the rms scatter of the intensity data along the fitted ellipse. Besides, the surface photometries at radii beyond where the ellipticity and PA cannot be measured, are obtained based on the last ellipticity and PA as the IRAF task ellipse is designed. The 80 points of this observed surface brightness profile are displayed in Fig. 3. We fitted King models (King 1966) to the surface brightness profiles. As usual, we parametrize the model with a core radius, r_c, a concentration index, $c = \log(r_t/r_c)$ (where r_t is the tidal radius), and a central surface brightness, $\mu(0)$. The fit was performed using a non-linear least-squares fit routine which uses the errors as weights. We derive a core radius $r_c = 0.21 \pm 0.01$ arcsec and a tidal radius $r_t = 21.78 \pm 1.06$ arcsec, the combination of which implies a concentration index $c = \log(r_t/r_c) = 2.01 \pm 0.02$. The central surface brightness is 13.510 mag arcsec^{-2}. Fig. 3 shows the surface brightness profile and the best-fitting King model. We also calculated the half-light radius (the radius that contains half of the light in projection), $r_h = 1.73 \pm 0.07$ arcsec. Adopting a distance to M31 of 770 kpc (Meylan et al. 2001), the core radius, the half-light radius and the tidal radius are 0.78 ± 0.04 pc, 6.5 ± 0.3 pc and 80.7 ± 3.9 pc, respectively, including their 1σ errors.

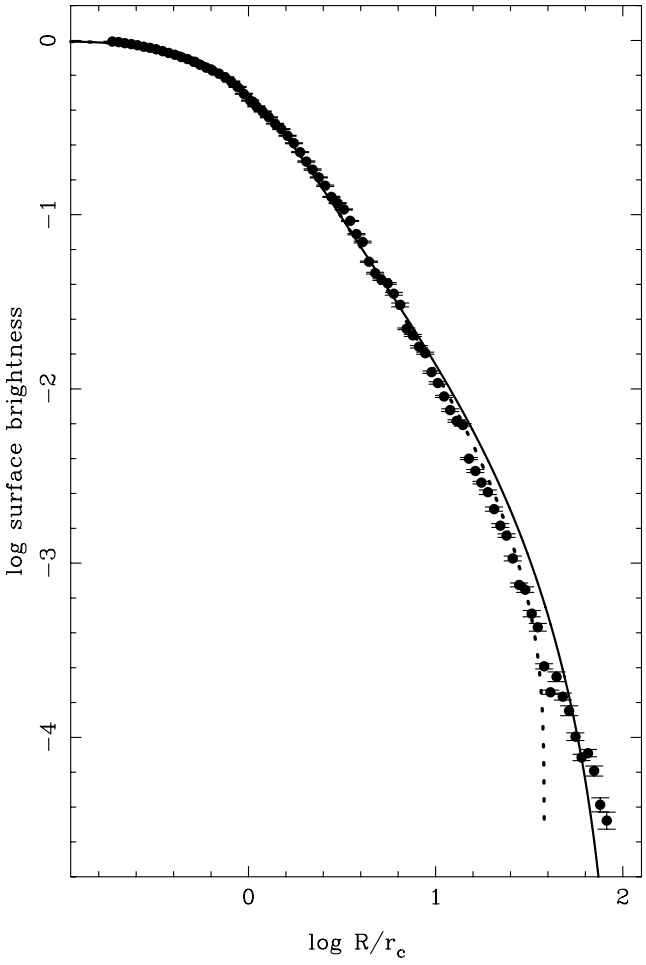

Figure 3. Surface brightness profile of G1 measured in the F555W passband. The solid line represents our best-fitting King model.

From Fig. 3, we can see that a King (1966) model does not fit the observed profile of G1 very well beyond 10 core radii. We note that we include all of the available data in our fits. Therefore, to guarantee the proper minimum χ^2 value, the observed profile at the outer tidal region must be considered. If we do this, the fit between 10 and 30 core radii is poor. On the other hand, the data at radii smaller than 30 core radii can be fitted well without considering the observed profile beyond 30 core radii, as indicated by the dashed line in Fig. 3. We thus conclude that a single-mass King (1966) model cannot fit the observed profile at the outer regions well. G1 is only the second GC in which convincing evidence for a real abundance dispersion has been seen, and combined with its high brightness (see details from Meylan et al. 2001, and references therein), it has been postulated as

the possible remnant core of a former dwarf elliptical galaxy which has lost most of its envelope through tidal interaction with its host galaxy. It may therefore be impossible to define its complex stellar and dynamical properties based on simple theories for GCs, such as King models. King models are based on the assumption that GCs are defined as single-mass, isotropic, lowered isothermal spheres. Although this assumption is simple, nearly all GCs can be fitted by King models (see details from Barmby et al. 2002; Larsen et al. 2002; McLaughlin & van der Marel 2005, and references therein). In fact, the structural parameters of nearly all GCs have been and continue to be determined on the basis of King models. However, for complicated stellar populations such as the stripped cores of a former dwarf galaxy, King models may not fit their profiles well in the tidal regions, due to the stronger tidal force of the host galaxy. However, we emphasize that Meylan et al. (2001) fitted the surface brightness profile of G1 with multimass King models, as defined by Gunn & Griffin (1979); the result was extremely good. Meylan et al. (2001) use four free parameters, in addition to an initial mass function (IMF) exponent: (i) the core radius, (ii) the scale velocity, (iii) the central value of the gravitational potential and (iv) the anisotropy radius, beyond which the velocity dispersion tensor becomes increasingly radial. As Meylan et al. (2001) pointed out, good models are considered as such not only on the basis of the minimum χ^2 of the surface brightness fit, since the topology of the χ^2 of the surface has no unique minimum, but also on the basis of their predictions of the integrated luminosity and mass-to-light ratio of the clusters. Therefore, Meylan et al. (2001) first computed about 150 000 models to explore the parameter space defined by the IMF exponent, the central gravitational potential, and the anisotropy radius. They then selected 12 models with the lowest χ^2 and fulfilling the two requirements above. Since the velocity dispersion profile for G1 is reduced to one single value, that is, the central velocity dispersion, the models are not constrained strongly, and equally good fits are obtained for rather different sets of parameters. Meylan et al. (2001) emphasized that reliable results only relate to parameters such as the concentration and the total mass, but probably fail in any more detailed parameters.

2.4 Comparison to previous results

This cluster has been studied previously by Pritchet & van den Bergh (1984), Rich et al. (1996), Meylan et al. (2001) and Barmby et al. (2002). van den Bergh (1984) found that the brightest GCs in a number of cluster systems are also the flattest. To check this conclusion, Pritchet & van den Bergh (1984) measured the flattening of G1 in the *B* band, using the CCD camera on the Canada–France–Hawaii Telescope. Their results showed that G1 is quite flattened with $\epsilon = 0.22 \pm 0.02$ in the radial range between ∼3 and 10 arcsec. These authors also found that an empirical King model fitted the surface brightness distribution of G1 very well. Based on *HST*/WFPC2 imaging in F555W with G1 projected on to the PC (with a pixel size of 0.045 arcsec), Rich et al. (1996) presented photometry of G1, and determined the structural parameters with the single-mass King models (King 1966), $r_c = 0.170 \pm 0.011$ arcsec (0.54 ± 0.04 pc) and $r_t = 28.21 \pm 0.44$ arcsec (90.0 ± 1.4 pc), and $r_h = 0.70$ arcsec and the central surface brightness at $\mu(0) = 13.5$ mag arcsec^{-2}. Rich et al. (1996) found a mean ellipticity $\epsilon \simeq 0.25 \pm 0.02$, which they stated was constant to the core, with no isophote rotation (PA $= 122^\circ$). Rich et al. (1996) appear not to have corrected for the instrumental point spread function (PSF), and do not state which radial variable they used. Since their ellipticity and PA measurements are based on elliptical isophote fits, however, it is likely that the radii they use are in fact the projected semimajor axis radii as well. Also using *HST*/WFPC2 imaging in F555W, Meylan et al. (2001) published aperture photometry of G1, and determined the structural parameters with multimass King models as defined by Gunn & Griffin (1979) as follows: $r_c = 0.14$ arcsec (0.52 pc), $r_t \simeq 54$ arcsec (200 pc), $r_h = 3.7$ arcsec (14 pc), with a central surface brightness $\mu(0) = 13.47$ mag arcsec^{-2} and a concentration $c = \log(r_t/r_c) \simeq 2.5$. Although they do not state the uncertainties in their fits, they use different models to fit the cluster's surface brightness profile, so that the variation in the resulting parameters gives us an indication of the associated uncertainties: $\sigma_{r_c} \simeq 0.01$pc, $\sigma_{r_t} \simeq 20$pc, $\sigma_{r_h} \simeq 0.7$ pc and $\sigma_c \simeq 0.05$. The mean ellipticity of Meylan et al. (2001) is $\epsilon \simeq 0.2$. It is evident that, r_t and r_h of Meylan et al. (2001) are much larger than those suggested by Rich et al. (1996) and in this paper. The reason for this difference may be that Meylan et al. (2001) used multimass King models, whereas both Rich et al. (1996) and the present paper employed single-mass King models. However, Gunn & Griffin (1979) have suggested that it is reasonable for r_t in multimass models to differ by a factor of 2 from that in single-mass model (also see Barmby et al. 2002). Barmby et al. (2002) also determined the structural parameters of G1 with single-mass King models based on the archival *HST*/WFPC2 images in F555W. Their results showed that $r_c = 0.21$ arcsec, $r_t = 10.5$ arcsec, $r_h = 0.82$ arcsec, and yielded a central surface brightness $\mu(0) = 13.65$ mag arcsec^{-2}. The mean ellipticity was $\epsilon \simeq 0.20$. Barmby et al. (2002) used the effective radius [$R_e = (ab)^{1/2} = a(1-\epsilon)^{1/2}$] as the radial variable in the fits, and they also convolve the fitted model with the instrumental PSF. As Barmby et al. (2002) pointed out, the resulting scale radii are systematically larger (by 0.076 ± 0.013 arcsec) and the concentrations smaller (by 0.09 ± 0.02) than when fitting models without PSF convolution.

3 GLOBULAR CLUSTERS, STRIPPED CORES AND DWARF SPHEROIDAL GALAXIES

The distribution of stellar systems in the M_V versus log R_h plane can provide interesting information on the evolutionary history of these objects (e.g. van den Bergh & Mackey 2004; Mackey & van den Bergh 2005). From ground-based observations of the brightest objects in NGC 5128, the nearest giant elliptical galaxy, Gómez et al. (2006) concluded that 'clusters form a continuum in this diagram'. However, such a conclusion should be regarded with some caution because (i) the clusters in NGC 5128 were found to have characteristic half-light radii of 0.3 arcsec to 1 arcsec, which is only marginally larger than the 0.3 arcsec to 0.6 arcsec seeing affecting their observations. Furthermore, (ii) Gómez et al. (2006) estimated that roughly 10 per cent of the objects in their sample might actually be background elliptical galaxies. In view of these caveats we prefer to restrict our discussion of the distribution of objects in the M_V versus log R_h plane to systems for which we have access to well-resolved GC-like objects, as long as their stellar populations are older than a few times 10^9 yr.

Recently, van den Bergh & Mackey (2004) and Mackey & van den Bergh (2005) showed that in a plot of luminosity versus half-light radius, the overwhelming majority of GCs, in the Milky Way, the Magellanic Clouds, the Fornax and Sagittarius dwarf spheroidal galaxies (dSphs), lie below (or to the right) of the line

$$\log R_h(\mathrm{pc}) = 0.25 M_V(\mathrm{mag}) + 2.95. \quad (1)$$

Exceptions to this rule are massive clusters, such as M54 and ω Centauri in the Milky Way, and G1 in M31, which are widely believed (Zinnecker et al. 1988; Freeman 1993; Meylan et al. 2001)

to be the remnant cores of now defunct dwarf galaxies. Because the well-known giant GC NGC 2419 (van den Bergh & Mackey 2004) in the Galaxy and 037-B327 (Ma et al. 2006) in M31 also lie above this line, it has been speculated that these objects might also be the remnant cores of dwarf galaxies (but see de Grijs, Wilkinson & Tadhunter 2005, for doubts regarding NGC 2419). However, more recently a number of large, but somewhat fainter clusters in M31 and NGC 6822 were found to be located above equation (1) as well (Huxor et al. 2005; Hwang et al. 2005; Mackey et al. 2006). This raises the question as to whether there might exist an entire class of objects which, in the M_V versus log R_h plane, are located between true GCs and dSphs, for which M_V and R_h values were published recently by McConnachie & Irwin (2006). Some support for this speculation is provided by the observations of M_V versus log R_h for the 14 brightest clusters in the peculiar nearby giant elliptical NGC 5128 (Martini & Ho 2004). These authors speculate that these brightest NGC 5128 GCs might be nucleated dwarf galaxies, based on their large masses and the observation by Harris et al. (2002) that some show extended envelopes. In addition, the apparently new class of ultracompact dwarf galaxies (UCDs) in the Fornax cluster (e.g. Mieske, Hilker & Infante 2002) also occupy a similar section of parameter space.

With the updated value of R_h for G1 from this paper, we present a plot of M_V versus log R_h in Fig. 4, in which M_V was taken from Meylan et al. (2001). It is evident that, with the updated R_h, G1 is still seen to lie above and brightward of the line defined by equation (1) (Mackey & van den Bergh 2005). Combined with the results of Meylan et al. (2001) that there exists an intrinsic metallicity dispersion amongst the stars of G1, this strengthens the conclusion that G1 may be the stripped core of a former dwarf galaxy (see details from Meylan et al. 2001; Mackey & van den Bergh 2005). Furthermore, and for completeness, in Fig. 4 we have also included the newly discovered Milky Way companions, based on Sloan Digital Sky Survey (SDSS) data. These include the objects found by Belokurov et al. (2006; four probable new dwarf galaxies and one unusually extended GC, Segue 1), a faint old stellar system at a distance of ∼150 kpc (Sakamoto & Hasegawa 2006), which might either be a new dwarf galaxy or an extended GC, an old, metal-poor stellar system at a distance of 45 ± 10 kpc (Willman et al. 2005a), which is either an unusual GC or an extreme dwarf satellite, two new dwarf satellites, one in the constellation of Ursa Major (Willman et al. 2005b), and another in the constellation of Canes Venatici (Zucker et al. 2006a), a faint new satellite in the constellation of Bootes at a distance of ∼60 kpc (Belokurov et al. 2006), and the faintest known satellite galaxy in the constellation of Ursa Major (Zucker et al. 2006b), which was subsequently confirmed with Subaru imaging, and an unusual dwarf galaxy in the outskirts if the Milky Way, which lies at a distance of ∼420 kpc (Irwin et al. 2007). Finally, the figure also includes the remote M31 GC B154 (Galleti et al. 2006), for which S. Galleti kindly provided us with its half-light radius, $r_\mathrm{h} \simeq$ 1.64 arcsec.

These results might be taken to suggest (see Fig. 4 and Table 3) that dwarf dSphs, stripped cores like ω Centauri, and normal GCs either form a continuum in the M_V versus log R_h plane, or – as seems to be the case based on the current best available data – that the data hint at a possible dichotomy between GCs and stripped dSph cores on one hand, and genuine dSphs on the other. A possible argument supporting latter point of view is that some dSphs, such as Fornax and Sagittarius, have their own systems of GC companions. Thus, taken at face value, this result strongly suggests that dSphs and GCs form systems of different order. Additional arguments in favour of this view are that (i) all dSphs appear to contain large amounts of dark matter, whereas such dark matter seems to be absent from GCs (Pryor et al. 1989; Moore 1996).

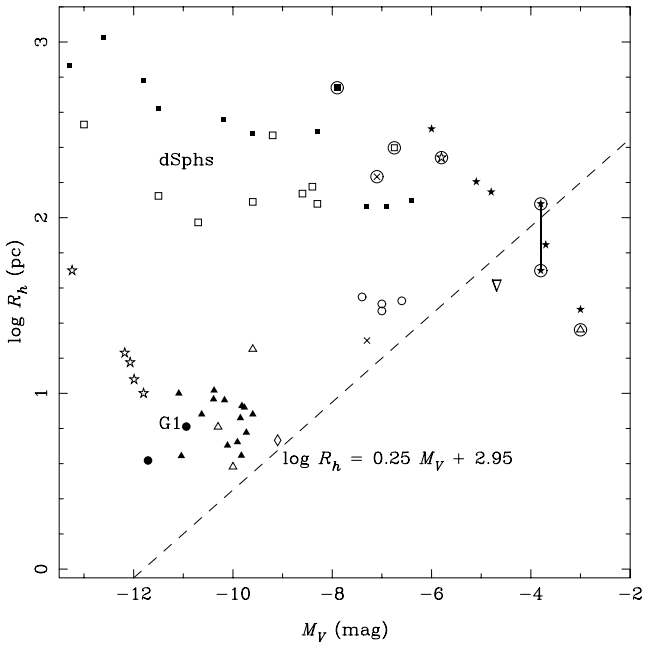

Figure 4. M_V versus R_h for GCs in M31 (037-B327 and G1: filled circles; B154: open diamond), Huxor et al. (2005) and Mackey et al. (2006)'s new faint large clusters in M31 (open circles), Galactic dSphs (Irwin & Hatzidimitriou 1995, open squares), putative Galactic stripped dSph cores (Mackey & van den Bergh 2005, open triangles), the newly discovered Milky Way companions (Belokurov et al. 2006: filled stars; Sakamoto & Hasegawa 2006: open upside down triangle; Willman et al. 2005a: circled triangle; Willman et al. 2005b: circled open square; Zucker et al. 2006a: circled filled square; Belokurov et al. 2006: circled open star; Zucker et al. 2006a: circled filled star; Irwin et al. 2007: circled cross), NGC 6822 GC (Hwang et al. 2005, cross), dSphs associated with the Andromeda galaxy (Harbeck et al. 2005; McConnachie & Irwin 2006; Martin et al. 2006, filled squares), UCDs in the Fornax cluster (Mieske et al. 2002, stars), and the brightest GCs in NGC 5128 (Martini & Ho 2004, filled triangles). Also shown is the line defined by equation (1), which gives the upper bound to the location of normal GCs in the M_V versus log R_h plane. The question as to whether or not the objects shown in this plot form a continuum is discussed in Section 4 of the present paper.

However, a weakness of this argument is that dark matter that once may have surrounded GCs might have been stripped from them by tidal interactions (e.g. Saito et al. 2006). Furthermore, (ii) individual stars in GCs (with the notable exceptions of ω Centauri, M54 and possibly M22 in the Galaxy and G1 in M31) all have similar metallicities, whereas individual stars in dSphs exhibit a wide range in [Fe/H] values. Finally, Pritzl, Venn & Irwin (2005) noted that the [α/Fe] and light r-process element ratios in most GCs mimic those in stars of similar metallicity in the Galactic field, and differ from those in dwarf galaxies. Thus, the apparent dichotomy in the M_V versus log R_h plane shown in Fig. 4 might well be a distinction in dark matter content and approximate co-evality of the stellar content of these objects. This view is supported by the observation that while the vast majority of Galactic and Magellanic Cloud GCs are very nearly coeval, there are indeed clear metallicity spreads in the objects lying above the dividing line.

It has also been claimed (Carraro et al. 2006) that the very old and metal-rich open cluster NGC 6791 might be the remnant core of a dSph galaxy as well. However, arguments against this hypothesis

Table 3. Data on globular clusters and dwarf galaxies.

Object	M_V	R_h	Reference
N2419	−9.6	17.88 pc	Galaxy: Mackey & van den Bergh (2005)
N5139	−10.3	6.44	
N6715	−10.0	3.82	
Carina	−8.6	137 pc	Irwin & Hatzidimitriou (1995)
Draco	−8.3	120	
Fornax	−13.0	339	
Leo I	−11.5	133	
Leo II	−9.6	123	
Sculptor	−10.7	94	
Sextans	−9.2	294	
Ursa Minor	−8.4	150	
Coma Berenices	−3.7	70 pc	New satellites of the Milky Way: Belokurov et al. (2007)
Canes Venatici II	−4.8	140	
Segue 1	−3.0	30	
Hercules	−6.0	320	
Leo IV	−5.1	160	
SDSS J1257+3419	−4.8	38 pc	A faint old system: Sakamoto & Hasegawa (2006)
B327	−11.71	4.15 pc	M31: Ma et al. (2006)
G1	−10.94	6.5 pc	M31: M_V from Meylan et al. (2001), and R_h from This paper
B514	−9.1	5.41 pc	M31: Galleti et al. (2006)
EC1	−7.4	35.4 pc	M31: Huxor et al. (2005) and Mackey et al. (2006)
EC2	−7.0	29.5	
EC3	−7.0	32.3	
EC4	−6.6	33.7	
SC1	−7.3	20 pc	NGC 6822: Hwang et al. (2005)
And I	−11.8	0.60 kpc	M31 companions: McConnachie & Irwin (2006)
And II	−12.6	1.06	
And III	−10.2	0.36	
And V	−9.6	0.30	
And VI	−11.5	0.42	
And VII	−13.3	0.74	
And IX	−8.3	0.31 kpc	M31 companion: Harbeck et al. (2005)
And XI	−7.3	115 pc	M31 companions: Martin et al. (2006)
And XII	−6.4	125 pc	
And XIII	−6.9	115 pc	
SDSSJ1049+5103	−3.0	23 pc	Milky Way companion: Willman et al. (2005a)
Ursa Major	−6.75	250 pc	New dwarf galaxy of the Milky Way: Willman et al. (2005b)
Canes Venatici	−7.9	550 pc	New dwarf satellite of the Milky Way: Zucker et al. (2006a)
Boötes	−5.8	220 pc	New faint satellite of the Milky Way: Belokurov et al. (2006)
Ursa Major II	−3.8	50 or 120 pc	New curious satellite of the Milky Way: Zucker et al. (2006b)
Leo T	−7.1	171 pc	An unusual dwarf galaxy in the outskirts of the Milky Way: Irwin et al. (2007)

include: (i) with [M/H] = 0.39 ± 0.05, NGC 6791 would be much more metal-rich than any other nearby putative stripped dwarf galaxy core, (ii) the small number of cluster stars for which metallicities have thus far been determined do not exhibit a significant metallicity spread. In this respect, this object would therefore differ from ω Centauri and a number of dSph companions to the Galaxy. Finally, (iii) it has been suggested by van den Bergh (2000, p. 54, and references therein) that NGC 6791 was originally a cluster in the metal-rich Galactic bulge that was ejected into the disc by tidal interactions with the massive bar believed to be located within the Galactic bulge. Further support for this suggestion has recently been provided by means of accurate, high spatial resolution proper motion measurements based on multi-epoch *HST*/ACS imaging (Bedin et al. 2006). Some light might be shed on this question if the values of M_V and R_h were available for NGC 6791. This might allow one to see if NGC 6791 falls above, or below the line in the M_V versus log R_h plane defined by equation (1).

In summary it is concluded that the sample of objects that can be reliably placed in the M_V versus log R_h diagram is still too small to decide whether this plane is normally occupied by a continuum of objects, or if unusual conditions such as 'tidal thrashing' are required to fill some regions of this plane. In this connection we note that the four UCDs in the Fornax cluster (De Propris et al. 2005) for which M_V and R_h values are available (all of which are located within 30 arcmin = 150 kpc of NGC 1399), lie in a compact grouping near $\langle M_V \rangle = -11.75$, $\langle \log R_h \rangle = 1.25$. In Fig. 4, this places

these objects near the centre of the apparent 'zone of avoidance' between the Local Group dSphs and the putative stripped cores of dwarf galaxies, which extends up to ∼0.7 dex above the line defined by equation (1). Similarly, Hasegan et al. (2005) have found three objects in the core of the Virgo cluster near M87 that lie between the regions in the M_V versus log R_h diagram that are usually occupied by normal dSphs and GC-like objects that are thought to be the stripped cores of such dSphs.

Finally, as has been pointed out by McConnachie & Irwin (2006), it is also puzzling that there appears to be a systematic difference between the locations of Galactic and Andromeda dSphs in the M_V versus log R_h plane.

4 SUMMARY

In this paper, we redetermined the structural parameters of Mayall II = G1 based on an F555W image obtained with the Advanced Camera for Surveys on the *HST*, by performing a fit to the surface brightness distribution of a single-mass isotropic King model. This allowed us to probe to smaller radii than ever before, thanks to the significantly higher spatial resolution offered by our instrumental set-up compared to that used by previous authors. We derive a core radius, $r_c = 0.21 \pm 0.01$ arcsec (=0.78 ± 0.04 pc), a tidal radius, $r_t = 21.78 \pm 1.06$ arcsec (=80.7 ± 3.9 pc), and a concentration index $c = \log\ (r_t/r_c) = 2.01 \pm 0.02$. The central surface brightness is 13.510 mag arcsec^{-2}. We calculate the half-light radius, at r_h = 1.73 ± 0.07 arcsec (=6.5 ± 0.3 pc). The results show that, within 10 core radii, a King (1966) model fits the surface brightness distribution well, although a single-mass King model cannot fit the observed profile at the outer regions well. The reason for this may be that for G1, which has been considered as the possible remnant core of a former dwarf elliptical galaxy, it is impossible to model the complicated stellar and dynamical properties based on simple theories for GCs, such as King models. This applies in particular to the outer regions, where there exist strong tidal force due to the host galaxy. We also discussed the variation of ellipticity and PA, and of surface brightness for the core of the object, in relation to previous measurements. We find that G1 falls in the same region of the M_V versus log R_h plane as ω Centauri, M54 and NGC 2419 in the Galaxy. All three of these objects have been claimed to be the stripped cores of now defunct dwarf galaxies. We discussed in detail whether GCs, nucleated dSph cores and normal dwarf galaxies form a continuous distribution in the M_V versus log R_h plane, or if GCs and dSphs constitute distinct classes of objects; we have presented arguments in favour of this latter option.

ACKNOWLEDGMENTS

This paper is based on observations made with the NASA/ESA *HST*, obtained at the Space Telescope Science Institute, which is operated by AURA, Inc., under NASA contract NAS 5-26555. These observations are associated with proposal 9767. RdG acknowledges an International Outgoing Short Visit grant to the National Astronomical Observatories of China in Beijing from the Royal Society. We are indebted to the referee for his/her thoughtful comments and insightful suggestions that improved this paper greatly. We are also indebted to Narae Hwang for providing us with his data on three GCs in the outer regions of NGC 6822 in advance of publication. Thanks are also due to Eva Grebel and Alan McConnachie for their help. We thank Silvia Galleti and Michele Bellazzini for providing us with the half-light radius measurements for B154 prior to publication. This research has made use of the Astrophysical Integrated Research Environment (AIRE), which is operated by the Centre for Astrophysics, Tsinghua University. This work was supported by the Chinese National Natural Science Foundation Grants Nos 10473012, 10573020, 10633020, 10673012 and 10603006.

REFERENCES

Barmby P., Holland S., Huchra J., 2002, AJ, 123, 1937
Battistini P., Bònoli F., Braccesi A., Federici L., Fusi Pecci F., Marano B., Börngen F., 1987, A&AS, 67, 447
Bedin L. G., Piotto G., Carraro G., King I. R., Anderson J., 2006, A&A, 460, L27
Belokurov V. et al., 2006, ApJ, 674, L111
Belokurov V. et al., 2007, ApJ, 654, 897
Carraro G., Villanova S., Demarque P., McSwain M. V., Piotto G., Bedin L. R., 2006, ApJ, 643, 1151
Da Costa G. S., Armandroff T. E., 1995, AJ, 109, 2533
de Grijs R., Wilkinson M. I., Tadhunter C. N., 2005, MNRAS, 361, 311
De Propris R., Phillipps S., Drinkwater M. J., Gregg M. D., Jones J. B., Evstigneeva E., Bekki K., 2005, ApJ, 623, L105
D'Onofrio M., Capaccioli M., Wagner S. J., Hopp U., 1994, Mem. Soc. Astron. Ital., 65, 731
Freeman K. C., 1993, in Dejonghe H., Habing H. J., eds, IAU Symp. 153, Galactic Bulges. Kluwer, Dordrecht, p. 263
Fusi Pecci F., Cacciari C., Federici L., Pasquali A., 1993, in Smith G. H., Brodie J. P., eds, ASP Conf. Ser. Vol. 48, The Globular Cluster–Galaxy Connection. Astron. Soc. Pac., San Francisco, p. 410
Galleti S., Federici L., Bellazzini M., Buzzoni A., Pecci F. F., 2006, ApJ, 650, L107
Gebhardt K., Rich R. M. R., Ho L. C., 2002, ApJ, 578, L41
Gebhardt K., Rich R. M. R., Ho L. C., 2005, ApJ, 634, 1093
Gómez M., Geisler D., Harris W. E., Richtler T., Harris G. L. H., Woodley K. A., 2006, A&A, 447, 877
Gunn J. E., Griffin R. F., 1979, AJ, 84, 753
Harbeck D., Gallagher J. S., Grebel E. K., Koch A. Z., Daniel B., 2005, ApJ, 623, 159
Harris W. E., 1991, ARA&A, 29, 543
Harris W. E., Harris G. L. H., Holland S. T., McLaughlin D. E., 2002, AJ, 124, 1435
Hasegan M. et al., 2005, ApJ, 627, 203
Huxor A. P., Tanvir N. R., Irwin M. J., Ibata R., Collett J. L., Ferguson A. M. N., Bridges T., Lewis G. F., 2005, MNRAS, 360, 1007
Hwang N., et al., 2005, in Jerjen H., Bingelli B., eds, IAU Colloquium No. 198, Near Field Cosmology with Dwarf Elliptical Galaxies, preprint (astro-ph/0510802)
Irwin M., Hatzidimitriou D., 1995, MNRAS, 277, 1354
Irwin M. et al., 2007, ApJ, 656, L13
King I., 1962, AJ, 67, 471
King I., 1966, AJ, 71, 64
Larsen S. S., Brodie J. P., Sarajedini A., Huchra J. P., 2002, AJ, 124, 2615
Lupton R. H., 1989, AJ, 97, 1350
Ma J. et al., 2006, ApJ, 636, L93
Mackey A., van den Bergh S., 2005, MNRAS, 360, 631
Mackey A. D. et al., 2006, ApJ, 653, L105
Martin N. F., Ibata R. A., Irwin M. J., Chapman S., Lewis G.F., Ferguson A. M. N., Tanvir N., McConnachie A. W., 2006, MNRAS, 371, 1983
Martini P., Ho L. C., 2004, ApJ, 610, 233
Mayall N. U., Eggen O. J., 1953, PASP, 65, 24
McConnachie A. W., Irwin M. J., 2006, MNRAS, 365, 1263
McLaughlin D. E., van der Marel R. P., 2005, ApJS, 161, 304
Meylan G., Heggie D., 1997, A&AR, 8, 1
Meylan G., Sarajedini A., Jablonka P., Djorgovski S., Bridges T., Rich R., 2001, AJ, 122, 830
Michie R. W., 1963, MNRAS, 125, 127
Mieske S., Hilker M., Infante L., 2002, A&A, 383, 823
Monaco L., Pancino E., Ferraro F. R., Bellazzini M., 2004, MNRAS, 349, 1278

Moore B., 1996, ApJ, 461, L13
Pritchet C., van den Bergh S., 1984, PASP, 96, 804
Pritzl B. J., Venn K. A., Irwin M., 2005, AJ, 130, 2140
Pryor C., McClure R. D., Fletcher J. M., Hesser J. E., 1989, AJ, 98, 596
Racine R., 1991, AJ, 101, 865
Riess A., 2003, ACS Instrument Science Report 2003-009
Riess A., Mack J., 2004, ACS Instrument Science Report 2004-006
Rich R. M., Mighell K. J., Freedman W. L., Neill J. D., 1996, AJ, 111, 768
Saitoh T. R., Koda J., Okamoto T., Wada K., Habe A., 2006, ApJ, 640, 22
Sakamoto T., Hasegawa T., 2006, ApJ, 653, L29
Sarajedini A., Layden A. C., 1995, AJ, 109, 1086
Sargent W. L. W., Kowal C. T., Hartwick F. D. A., van den Bergh S., 1977, AJ, 82, 947
Sirianni M. et al., 2005, PASP, 117, 1049
Staneva A., Spassova N., Golev V., 1996, A&AS, 116, 447
van den Bergh S., 1984, PASP, 96, 329
van den Bergh S., 1996, Observatory, 116, 103
van den Bergh S., 2000, The Galaxies of the Local Group. Cambridge Univ. Press, Cambridge
van den Bergh S., Mackey A. D., 2004, MNRAS, 354, 713
Willman B. et al., 2005a, AJ, 129, 2692
Willman B. et al., 2005b, ApJ, 626, L85
Zucker D. B. et al., 2006a, ApJ, 643, L103
Zucker D. B. et al., 2006b, ApJ, 650, L41
Zinnecker H., Keable C. J., Dunlop J. S., Cannon R. D., Griffiths W. K., 1988, in Grindlay J. E., Philip A. G. D., eds, Proc. IAU Symp. 126, The Harlow-Shapley Symposium on Globular Cluster Systems in Galaxies. Reidel, Dordrecht, p. 603

This paper has been typeset from a TEX/LATEX file prepared by the author.